applied sciences

MDPI

Article

Green Hydrogen Production—Fidelity in Simulation Models for Technical–Economic Analysis

Adrián Criollo [1,2], Luis I. Minchala-Avila [1], Dario Benavides [3], Danny Ochoa-Correa [1], Marcos Tostado-Véliz [3,*], Wisam Kareem Meteab [3] and Francisco Jurado [3]

[1] Department of Electrical Engineering, Electronics, and Telecommunications (DEET), Universidad de Cuenca, Cuenca 010101, Ecuador; adrian.criollor@ucuenca.edu.ec (A.C.); ismael.minchala@ucuenca.edu.ec (L.I.M.-A.); danny.ochoac@ucuenca.edu.ec (D.O.-C.)
[2] Department of Electrical Maintenance and Industrial Control, Instituto Superior Tecnológico del Azuay, Cuenca 010105, Ecuador
[3] Department of Electrical Engineering, University of Jaén, 23700 Linares, Spain; djbenavi@ujaen.es (D.B.); wkm00001@red.ujaen.es (W.K.M.); fjurado@ujaen.es (F.J.)
* Correspondence: mtostado@ujaen.es

Abstract: Green hydrogen production is a sustainable energy solution with great potential, offering advantages such as adaptability, storage capacity and ease of transport. However, there are challenges such as high energy consumption, production costs, demand and regulation, which hinder its large-scale adoption. This study explores the role of simulation models in optimizing the technical and economic aspects of green hydrogen production. The proposed system, which integrates photovoltaic and energy storage technologies, significantly reduces the grid dependency of the electrolyzer, achieving an energy self-consumption of 64 kWh per kilogram of hydrogen produced. By replacing the high-fidelity model of the electrolyzer with a reduced-order model, it is possible to minimize the computational effort and simulation times for different step configurations. These findings offer relevant information to improve the economic viability and energy efficiency in green hydrogen production. This facilitates decision-making at a local level by implementing strategies to achieve a sustainable energy transition.

Keywords: electrolyzer; proton exchange membrane; fuel consumption; opal-RT; real-time simulation; green hydrogen

Citation: Criollo, A.; Minchala-Avila, L.I.; Benavides, D.; Ochoa-Correa, D.; Tostado-Véliz, M.; Meteab, W.K.; Jurado, F. Green Hydrogen Production—Fidelity in Simulation Models for Technical–Economic Analysis. *Appl. Sci.* **2024**, *14*, 10720. https://doi.org/10.3390/app142210720

Academic Editor: Seung-Hoon Yoo

Received: 22 October 2024
Revised: 11 November 2024
Accepted: 18 November 2024
Published: 19 November 2024

1. Introduction

In recent years, hydrogen energy has gradually become a new alternative for clean energy generation. The multiple applications of hydrogen as a means of energy storage in the energy sector, transport, industry, and various other applications have generated great interest in global economic development [1], thus allowing a promising alternative to satisfy and maintain global energy needs with a sustainable tendency [2–5]. As a result, hydrogen generation has sparked great interest in some countries as a fuel of the future [6–8]. However, ensuring green hydrogen production from a renewable energy perspective presents significant challenges. Renewable energy sources (RESs) are naturally variable, requiring energy storage systems (ESSs) to accommodate daily and seasonal changes. Currently, the search for methods and technological development in new energy storage systems is ongoing. One of the processes for generating green hydrogen is through the electrolysis of water using RESs. Recently, there has been significant research and development into this technology, and various methods have been developed to increase efficiency and reduce production costs [9]. Therefore, this article analyzes and studies green hydrogen production in a micro-grid case study based on medium- and high-precision models for a feasible technological and economic analysis. Green hydrogen is generated

through an electrolyzer, which is composed of a photovoltaic (PV) system as a renewable resource and an ESS to reduce energy consumption from the electrical grid.

Techno-economic analyses have been fundamental in determining the payback period of investments. However, more studies are currently needed to analyze the return on investment when using excess solar energy to charge energy vectors such as hydrogen. One solution is to produce hydrogen through the electrolysis—splitting with an electric current—of water and to use that hydrogen in a fuel cell (FC) to produce electricity during times of low power production or peak demand or to use the hydrogen in fuel cell vehicles. In addition, hydrogen is a non-toxic and clean energy carrier with a specific energy of 141.9 kJ/g, compared to 46.5 kJ/g of gasoline [10,11]. However, it is important to consider the high cost that its production could generate, so several optimization studies have been carried out. For example, one study has optimized a solar energy system to electrify Kousseri, Cameroon, comparing four algorithms for sizing systems in isolated grids [12]. Similarly, ref. [13] presents the design of a hybrid photovoltaic (PV)/wind turbine (WT)/FC system for three regions in Iran, using the whale optimization algorithm (WOA) to minimize the net present value of the hybrid system while meeting the probability of power generation losses. Furthermore, a study presents a hybrid renewable energy system for domestic and telecommunications loads across India, considering technical, economic, environmental, and social factors [14]. Among the findings, Chennai emerges as the optimal location for domestic and telecommunications loads based on analyses of cost of energy (COE), total net present cost (TNPC), annualized cost of system (ACS), carbon emissions (CEs), and particulate matter (PM), compared to New Delhi and Mumbai.

On the other hand, ref. [15] examines the feasibility of using wind and solar plants for hydrogen generation via electrolysis, focusing on component sizing and the location's impact on the levelized cost of hydrogen. A notable aspect of the research is their finding that hydrogen shows a negative correlation with the amount of electrical production surplus. Similarly, a study analyzed the production of green hydrogen in Paraguay [16]. This study obtained a total production potential of 22.5×10^6 tons/year, which favors the incorporation of the hydrogen economy in the automotive transportation and residential energy sectors. Proton exchange membrane water electrolyzer (PEMWE) technologies boast higher current densities (1–2 Acm^{-2}) than alkaline water electrolyzers (AWEs) and produce a higher purity of hydrogen up to 99.9999% [17]. Barriers associated with those systems have been gathered and recapped to identify key solutions that could aid in their removal. Likewise, in a study, the results found that a 4.2% reduction in the amount of electrical energy needed for electrolysis showed that barriers to solar hydrogen generation are related to the industry of PV cells, atmospheric conditions affecting PV cells' performance, and those related to solar-to-hydrogen (STH) production and storage [18]. According to [19], by connecting a solar module with the voltage at its maximum power point (Vmpp) to a high-efficiency PEM electrolyzer, the group was able to achieve a solar-to-hydrogen efficiency of 12.4%, compared to a past system that only reached 2–6%. This study utilized a 20-cell PEM electrolyzer stack and various PV modules with different output voltages and current levels.

In this context, the modeling of large-sized electrolyzers has also been studied for real-time simulation and the possibility of frequency support by electrolyzers [20]. Also, electrolyzers have been found to support frequency stability more effectively than conventional generators, benefiting the power system's stability. The development of a generic electrolyzer model has allowed simulations to analyze the impact of electrolyzers on power system stability, showing promising results. Field measurements and simulations have validated the model's ability to replicate the behavior of real electrolyzers, highlighting their potential to support frequency and voltage stability in future power systems. In the same line, the reference [21] explores the impact of the operational constraints and the control strategies on the effectiveness of hydrogen electrolyzers in providing frequency control services; the results show that hydrogen electrolyzers can effectively contribute to helping prevent widespread load shedding in power systems. Also, in the studies carried

out by [22,23], the results present that proton exchange membrane hydrogen electrolyzer units are a suitable candidate for virtual inertia response, regulation, and contingency frequency control ancillary services, potentially replacing the need for battery installations in future power systems. Electrolyzers can regulate power off-take based on grid frequency. A techno-economic model optimizes revenue by considering power band and ancillary services. Operating the electrolyzer at optimal values maximizes revenue. Offering symmetric primary reserve is a valid option for revenue generation [24].

On the other hand, high-fidelity mathematical models used to perform simulations in the fields of chemical engineering and fluid dynamics can take hours or even days to simulate due to the large amount of data and parameter tuning required in these models. To address these challenges, high-fidelity component-level models can be replaced with reduced-order models that balance accuracy in exchange for lower computational complexity. To create a static reduced-order modeling ROM, curve fitting, look-up tables, and neural networks can be used to create a suitable model [25,26]. This could directly influence the time required for the simulation process of the electrolyzer and the micro-grid system. Therefore, the point of interest is specifically to analyze the energy production and determine the amount of hydrogen that can be produced. Parameters must be taken into account for a technical–economic study.

Consequently, all these factors represent a gap in research for the generation of green hydrogen. Some studies present technical–economic analyses for different countries, which do not allow the approach to be generalized due to the economic power of each one. In addition, there are different conditions for renewable resource generation. This study focuses on a case study to offer alternatives in the regulatory framework and the development and implementation of state support measures for hydrogen energy projects in countries undergoing sustainable development. Many studies in the literature have focused on hydrogen production solely with surplus renewable energy. However, the proposed system allows the generation of green hydrogen continuously throughout the year with minimal consumption from the electrical grid on days of low PV production. Furthermore, the management model achieves an adequate handling of the ESS, which allows for a daily energy balance in an autonomous manner. It also includes data and technical parameters of the equipment used during its experimentation, which brings its effectiveness closer to simulation models for small- and large-scale technical–economic studies. Based on these green hydrogen initiatives, the contributions of this article are as follows:

- A PV energy management and storage model for the uninterrupted production of green hydrogen through self-consumption is proposed.
- The replacement of the high-fidelity model of the electrolyzer with reduced-order modeling is studied based on real experimentation.
- A comparative study is carried out between the energy consumption of methane reforming to generate hydrogen versus the proposal developed with renewable energies.
- A technical–economic analysis is performed for the estimation of local hydrogen production versus the energy cost in kWh/kg.
- Data from experimental tests are used in a real-time simulation environment and micro-grid laboratory tests.

The remainder of this paper is organized as follows: Section 2 presents the details of the modeling of the system components, Section 3 presents the experimental phase with electrolytes, and Section 4 presents the case study, including simulation results and discussion. Finally, Section 5 concludes the study.

2. System Component Modeling

2.1. Production of Green Hydrogen

The production of green hydrogen through the electrolyzer results from the optimal performance of RESs and ESSs with minimal or no consumption from the electrical grid. Therefore, this study proposes the continuous production of hydrogen through electrolyzers. Figure 1 presents a generalized scheme for hydrogen production based on

photovoltaics with energy storage support, which covers a pre-established demand profile for the electrolyzer (ETZ). Excess PV energy is stored in the ESS to deliver the energy in case of shortages later. In this context, the PV power injected into the grid P_t^{PV} allows the supply of the demand of the electrolyzer P_t^{ETZ}. In the case of excess (−) or the absence (+) of generation, the power of the energy storage system P_t^{ESS} allows the energy management to be completed with the objective of reducing the power consumption of the electrical grid P_t^{Gd}. This function is defined in the following Equation (1):

$$min[P_t^{Gd} = P_t^{PV} \pm P_t^{ESS} - P_t^{ETZ}] \quad (1)$$

In this way, self-consumption is achieved from the demand side at the point of common coupling (PCC). Finally, hydrogen can be evaluated as an energy potential in the use of fuel cells.

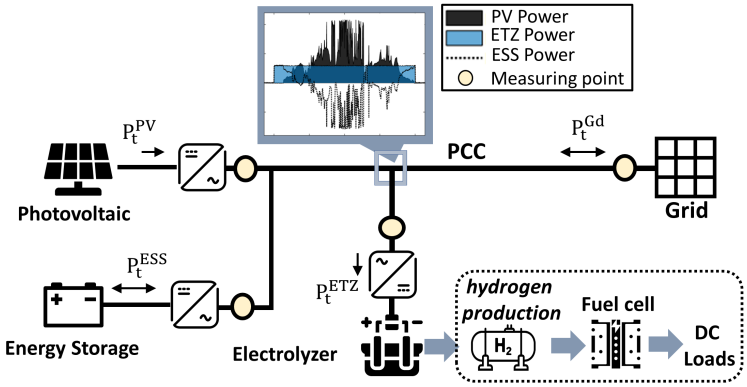

Figure 1. Scheme for hydrogen production based on photovoltaics with energy storage support.

2.2. Photovoltaic Array

The pre-established photovoltaic modules of the system advisor model of the National Renewable Energy Laboratory (NREL) are used. Specifically, it was simulated with the Atersa A-250P model (Elecnor, Valencia, Spain) with a nominal power of 15 kWp based on the 15 × 4 (series–parallel) configuration [27,28]. The PV array is modeled with parameters that use a light-generated current source (I_L), a diode, a series resistor (R_s), and a shunt resistor (R_{sh}) to represent the I–V characteristics of the modules. These values depend on the input variables of irradiance (W/m^2) and temperature (ºC) [29]. The equations are detailed below:

$$I_d = I_0\left[exp(\frac{V_d}{V_T}) - 1\right] \quad (2)$$

where I_d is diode current (A), I_0 is diode saturation current (A), V_d is diode voltage (V), and the voltage V_T is calculated as follows:

$$V_T = \frac{kT}{q} \times nI \times Ncell \quad (3)$$

where k is the Boltzmann constant (1.3806 × 10^{-23} J· K^{-1}), T is the cell temperature (K), q is the electron charge (1.6022 × 10^{-19} C), nI is the diode ideality factor and $Ncell$ is the number of cells connected in series in a module. Below in Figure 2, the PV power produced $P = IV$ and the characteristic V–I curves are presented.

The operating ranges of the voltage of the PV system are 15 kWp under different levels of solar irradiation G (see Figure 2a). The maximum power tracking for the voltage is around 450 Vdc. Similarly, the nominal current of 36 A with different temperature values established in the model parameters is presented in Figure 2b. Finally, this model is integrated with a DC/DC converter and, subsequently, a DC/AC converter for connection to the PCC [28].

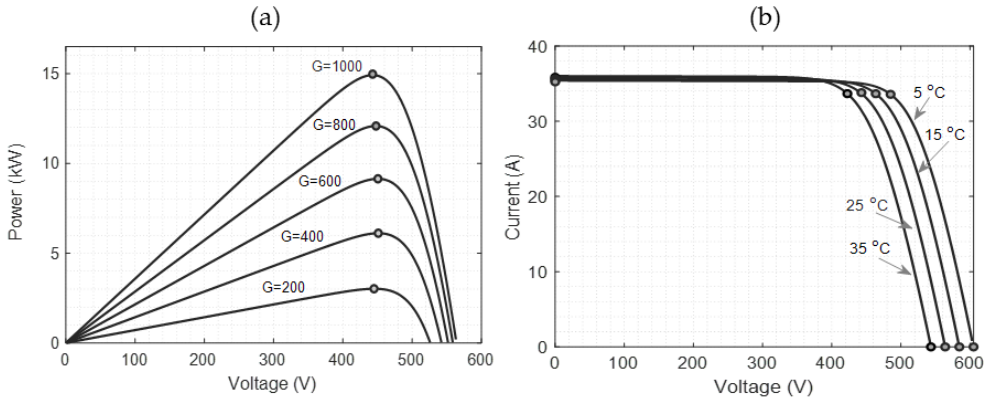

Figure 2. PV system model: (**a**) PV power, (**b**) I-V characteristics.

2.3. Electrolyzer Model

Electrolyzers can be modeled using various approaches. In this case, the chemical–electrical approach is adopted. The electrolyzer block represents the electrical load of the electrolyzer, which consists of an anode and a cathode separated by an electrolyte. This block calculates the hydrogen production based on the electrical energy input and the water temperature in the tank [30]. The electrolyzer block calculates the electrical power using Equation (4):

$$P_E = \frac{v^2}{R_T} \rightarrow P_t^{ETZ} \tag{4}$$

where v is the voltage and R_T is the total resistance given by Equation (5). The R_T, is defined by

$$\begin{aligned} \frac{1}{R_T} &= \frac{1}{R_{el}} + \frac{1}{R} \\ R_{el} &= \frac{\rho(pH) \times x}{A} \end{aligned} \tag{5}$$

where R is the external resistance, A is a resistive term obtained from the cross-sectional transport area, x is the anode–cathode distance, and $\rho(pH)$ is the electrical resistivity of the solution. The energy per mole stored over the electrical load facilitates water electrolysis and can be computed using Equation (6):

$$G_E = \frac{P_E}{\frac{1 \text{ mol}}{\text{s}}} \tag{6}$$

In performing electrolysis, the electrolyzer needs a minimum level of energy according to Equation (7):

$$G_{min} = \Delta H - \frac{T}{T_o} T_{\Delta s} \tag{7}$$

where ΔH is the water enthalpy, $T_{\Delta s}$ is the reaction entropy, T is the water temperature, and T_o is the reference temperature.

If there is not enough electrical energy to split the water molecules, the electrolyzer will not generate hydrogen. Consequently, the electrolyzer block determines Equations (8) and (9), the rates of electron, mole, and hydrogen production, respectively.

$$mol_e = \begin{cases} \frac{\mu(G_E - G_{min})}{e_V N_A} & G_e > G_{min} \\ 0 & G_e \leq G_{min} \end{cases} \tag{8}$$

$$mol_{H_2} = \begin{cases} \frac{N_c mole}{2} & G_e > G_{min} \\ 0 & G_e \leq G_{min} \end{cases} \tag{9}$$

where N_A is the Avogadro constant, e_V is the energy per electron, N_c is the number of cells, and μ is the temperature-dependent efficiency of the electrolysis.

The current passing through the electrolyzer tank, as given by Equation (10), is determined using the following expression, where F represents the Faraday constant (96,485.3321 s·A/mol):

$$i = mol_e \times F \tag{10}$$

The electrolyzer block computes the mass rates of water consumption and hydrogen production using Equations (11) and (12), respectively:

$$\dot{m}_{H_2O} = mol_{H_2} M_{H_2O} \tag{11}$$

$$\dot{m}_{H_2} = mol_{H_2} M_{H_2} \tag{12}$$

where M_{H_2O} is the molar mass of water, and M_{H_2} is the molar mass of hydrogen.

2.4. Application of Hydrogen as a Fuel Cell

2.4.1. Simplified Fuel Cell Model

The following model is generic and can emulate the behavior of any fuel cell type fed with hydrogen and air (see Figure 3). The approach involves extracting data from the data sheet to perform simulations without the need for experimental tests on an actual stack [31].

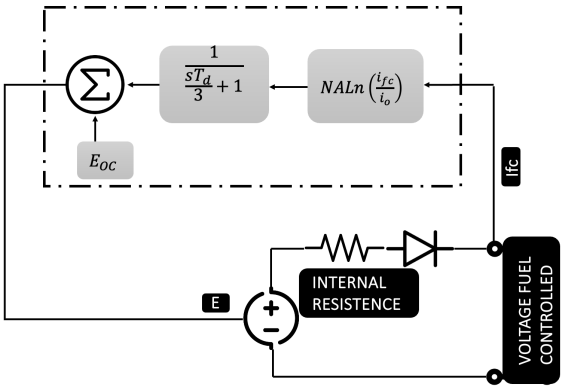

Figure 3. Simplified model representation of fuel cell.

Fuel cell models can be classified into three categories: chemical, experimental, and electrical. Chemical models include complex chemical and thermodynamic phenomena but require excessive parameters and cannot be easily added to electrical simulation programs [32–34]. Experimental models are derived from experiments and represent the fuel cell by look-up tables or empirical expressions [35,36]. Electrical models represent the fuel cell through electrical circuit elements [31]. There, the controlled voltage source E is given by Equation (13). It is important to note that E_{oc} represents open-circuit voltage, N the number of cells, A the Tafel slope, i_o the exchange current, T_d the response time at 95% of the final value in seconds, R_{ohm} the internal resistance, i_{fc} the FC current, and V_{fc} the FC voltage. Equation (14) refers to stack total voltage considering the losses due to electrodes and electrolytes [31].

$$E = E_{oc} - NAln\left[\left(\frac{i_{fc}}{i_o}\right) \times \frac{1}{\frac{sT_d}{3}+1}\right] \tag{13}$$

$$V_{fc} = E - R_{ohm} \times i_{fc} \tag{14}$$

2.4.2. The Detailed Fuel Cell Model

The detailed model accurately simulates a specific fuel cell stack by adjusting for changes in parameters such as pressure, temperature, composition, and flow rates of the fuel and air.

These variations influence the Tafel slope (A), the exchange current (i_0), and the open-circuit voltage (E_{oc}). The equivalent circuit of the detailed model (illustrated in Figure 4) is identical to that of the simplified model, except that the parameters (E_{oc}, i_0, A) need to be updated based on the input pressures, flow rates, stack temperature, and gas compositions [31].

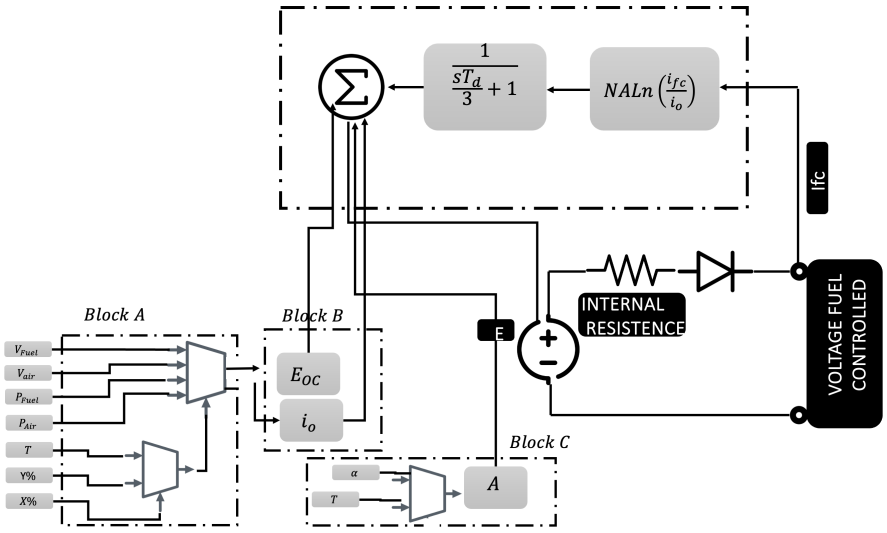

Figure 4. Detailed fuel cell stack model.

According to the detailed model, the next set of equations has been modified:

$$E_{oc} = K_C \times E_n \tag{15}$$

$$i_o = \frac{zFk(P_{H_2} + P_{O_2})}{Rh} \times \exp\left(\frac{-\Delta G}{RT}\right) \tag{16}$$

$$A = \frac{RT}{z \times \alpha \times F} \tag{17}$$

where R represents the unit of molar entropy, F the Faraday constant, z the number of moving electrons (two in this case), E_n the Nernst voltage, which is the thermodynamics voltage of the cells and depends on the temperatures and partial pressures of reactants and products inside the stack, α the charge transfer coefficient, P_{H_2} the partial pressure of hydrogen inside the stack, P_{O_2} the partial pressure of oxygen inside the stack, k Boltzmann's constant, h Planck's constant, ΔG the activation energy barrier, T the temperature of operation, and K_C the voltage constant at nominal conditions.

As illustrated in Figure 4, Blocks A, B, and C are used to calculate new values for E_{oc}, i_0, and A. Initially, Block A determines the conversion rates (utilization) of hydrogen (U_{fH_2}) and oxygen (U_{fO_2}) as follows:

$$U_{fH_2} = \frac{60000R \times Ti_{fc}}{z \times F \times P_{fuel} \times V_{fuel} \times x\%} \tag{18}$$

$$U_{fO_2} = \frac{60000R \times Ti_{fc}}{2 \times z \times F \times P_{air} \times V_{air} \times y\%} \tag{19}$$

In Equation (18), P_{fuel} represents the absolute supply pressure of fuel, P_{air} the absolute supply pressure of air, V_{fuel} the fuel flow rate, V_{air} the air flow rate, $x\%$ the percentage of hydrogen in the fuel, and $y\%$ the percentage of hydrogen in the oxidant.

Block B, shown in Figure 4, determines the partial pressures and the Nernst voltage as follows:

$$P_{H_2} = (1 - U_{fH_2}) \times x\% P_{fuel} \tag{20}$$

$$P_{O_2} = (1 - U_{fO_2}) \times y\% P_{air} \quad (21)$$

$$P_{H_2O} = (w + 2y\% \times U_{fO_2}) \times P_{air} \quad (22)$$

$$E_n = 1.299 + (T - 298) \times \frac{-44.43}{zF} + \frac{RT}{zF} \ln\left(P_{H_2} \times P_{O_2}^{1/2}\right) \quad (23)$$

for $T > 373$ K:

$$E_n = 1.299 + (T - 298) \times \frac{-44.43}{zF} + \frac{RT}{zF} \ln\left(\frac{P_{H_2 \times P_{O_2}^{1/2}}}{P_{H_2O}}\right) \quad (24)$$

In Equation (22), P_{H_2O} represents the partial pressure of water vapor and w the percentage of water vapor in the oxidant. The nominal value and Nernst voltage E_n can also be calculated from the Equation (24), where T represents temperature operation, R refers to the amount of energy needed to raise the temperature of one mole of a substance by one kelvin, and finally z is the number of moving electrons.

By knowing the partial pressures of gases and the Nernst voltage, the new values for the open-circuit voltage and the exchange current can be calculated using Equation (13) and (16), respectively. Block C then calculates the new Tafel slope value using Equation (17).

To model the effect of oxygen depletion (due to air compressor delay) on the stack voltage, parameters for flow dynamics such as the peak utilization (Uf_{O_2}(peak)) and the corresponding voltage undershoot (Vu) are needed. Oxygen depletion within the cell increases its utilization above the nominal value, and the Nernst voltage is subsequently adjusted as follows.

2.4.3. Model Assumptions and Limitations

The following assumptions and limitations have been considered in the development of the simulation:

- Gases are assumed to behave as ideal gases.
- The stack is supplied with hydrogen and air.
- A cooling system ensures stable temperatures at the cathode and anode exits, matching the stack temperature.
- A water management system maintains appropriate humidity levels within the cell under all load conditions.
- Pressure drops across flow channels are assumed to be negligible.
- Voltage drops within the cell are primarily due to reaction kinetics and charge transport, as fuel cells typically do not operate in the mass transport region.
- The cell's resistance is assumed to remain constant under all operating conditions.
- Gas or water flow through the membrane is not accounted for.
- The effects of membrane temperature and humidity on stack resistance are not considered.

2.5. Energy Storage Model

Energy storage systems have proven to be one of the leading solutions when there is a shortage of renewable energy generation in order to balance demand with generation. Its application is of great importance to achieve the correct performance of all elements in the electrical grid. In this context, the use of batteries is based on the production of green hydrogen with minimal or zero consumption from the grid. Excess PV energy is stored in the batteries during peak power production hours. Then, the accumulated energy is returned in the case of demand from the electrolyzer. This guarantees optimal performance for hydrogen production without interruption. Although each ESS depends on constructive and technological characteristics, the control of the SoC is exclusively detailed and can be applied to any ESS. Therefore, the SoC of the batteries is analyzed through simulation in the following way.

The ESS allows charging or discharging in random sequences with any amplitude between 0 and 100% of its effective capacity. The ESS control algorithm to limit the SoC is

shown in Figure 5, where the value of P_t^{ref} is initially assigned as the difference between the photovoltaic power P_t^{PV} and the electrolyzer demand power P_t^{ETZ}, in such a way that being a value greater than zero, it allows the charging of the P_t^{ESS} from a time $(\Delta t_{charge} = t_2 - t_1)$ in the positive cycle and defines $P_t^{charge} = P_t^{ref}$. Subsequently, the charge energy value Ec_t^{ESS} is calculated as the integral of the charge power. The same is applied for the discharge energy, assigned for the negative cycle Ed_t^{ESS}. The total energy of the ESS at E_t^{ESS} during a time t_n and t_n' varies as a function of the difference in the charge and discharge energy, respectively. This procedure is summarized in Equation (25):

$$\begin{cases} P_t^{ref} = P_t^{PV} - P_t^{ETZ} \\ Ec_t^{ESS} = \int_{t_1}^{t_2} P_t^{charge} dt \rightarrow P_t^{ref} \geq 0 \\ Ed_t^{ESS} = \int_{t_1'}^{t_2'} P_t^{discharge} dt \rightarrow P_t^{ref} < 0 \end{cases} \tag{25}$$

Then, the value of the total energy in the storage is calculated as follows:

$$E_t^{ESS} = \eta_c \times Ec_t^{ESS} - \frac{1}{\eta_d} \times Ed_t^{ESS} \tag{26}$$

where η_c is charging efficiency and η_d is discharging efficiency. Then, the calculation to determine the SoC is calculated with the maximum storage energy E_{max}, that is,

$$SoC_t^{ESS} = SoC_{t-1}^{ESS} + \frac{E_t^{ESS}}{E_{max}} \times 100\% \tag{27}$$

The SoC restriction is limited in its maximum SoC_{max} and minimum SoC_{min} values allowed according to the following equation:

$$\begin{cases} P_t^{ESS} = P_t^{ref} \rightarrow \left(SoC_{min} \leq SoC_t^{ESS} \leq SoC_{max}\right) \\ P_t^{ESS} = 0 \rightarrow \left(SoC_{max} < SoC_t^{ESS} < SoC_{min}\right) \end{cases} \tag{28}$$

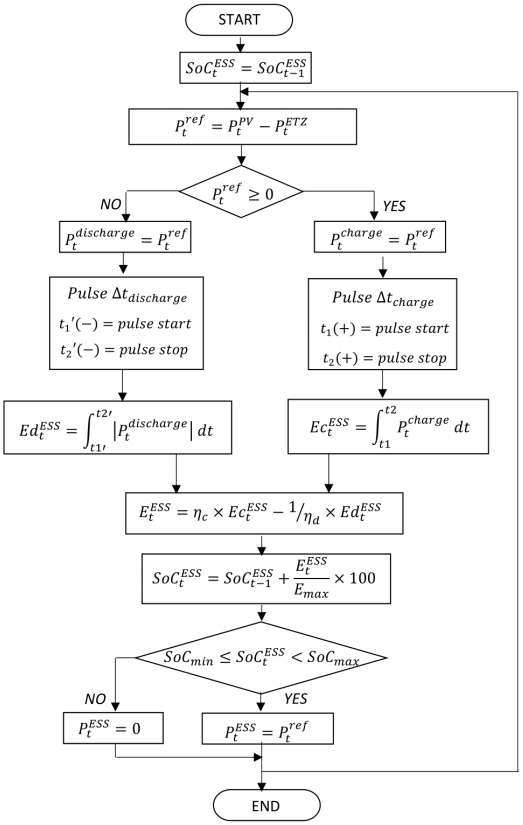

Figure 5. ESS state of charge control algorithm.

3. Experimental Phase with Electrolytes

During the experimental phase for obtaining hydrogen fuel by electrolysis of water, the research was based on the results of a preliminary study [37]. Initially, solutions were prepared with sodium hydroxide (NaOH) at a 1% concentration, sulfuric acid (H_2SO_4) at a 37% concentration, and sodium bicarbonate ($NaHCO_3$) at a 1% concentration. It is worth noting that the electrochemical analysis was carried out in the Laboratory of the Faculty of Chemical Sciences. The results are summarized in Table 1, which presents the outcomes of the experimentation with sulfuric acid for electrodes both with a size of 50 cm^2.

According to Figure 6a for an electrode area of 50 cm^2 and Figure 6b for an electrode area of 100 cm^2, it can be confirmed that at the moment hydrogen is generated, its weight is approximately double that of oxygen, as demonstrated by the graphs. Furthermore, as the distance between electrodes decreases from 39 cm to 1 cm, hydrogen production increases. In Figure 6a, there is a peak of 606 cubic centimeters (c.c.) at a concentration of 26.92%. Meanwhile, for Figure 6b, the maximum limit reaches 1217 c.c. at a concentration of 24.21%.

Based on the study of the ELS500 Hydrogen Generator electrolyzer of the Micro-Grid of the University of Cuenca, to prepare a 1% potassium hydroxide (KOH) solution in 4 L of water, we dissolved 40 g of KOH. This is based on the following Equation (29):

$$Concentration = \frac{\text{mass of solute}}{\text{volume of solution}} \times 100\% \quad (29)$$

For a 1% concentration, the mass of KOH should be 1% of the solution volume in milliliters (4000 mL), resulting in 40 g of KOH required to achieve the desired concentration in 4 L of water.

Table 1. Experimental results with H_2SO_4, electrode area 50 cm^2, electrolyte volume 2 lt, and stainless steel electrodes.

					Distance			**cm**									
			39	**30**	**20**	**10**	**1**	**39**		**30**		**20**		**10**		**1**	
								Vol (cc)		**Vol (cc)**		**Vol (cc)**		**Vol (cc)**		**Vol (cc)**	
°C	**%**	**F**		**Current**		**mA**		**H_2**	**O_2**	**H_2**	**O_2**	**H_2**	**O_2**	**H_2**	**O_2**	**H_2**	**O_2**
25	37.4	1.19	345	363	470	607	857	182	90	208	105	278	138	366	180	517	255
25	32.16	1.19	333	378	464	619	904	175	86	220	108	276	138	372	182	550	274
25	31.46	1.17	303	332	426	577	822	161	80	189	94	252	125	346	171	496	247
25	29.11	1.16	341	393	486	642	954	178	89	227	113	288	143	385	189	581	291
25	28.14	1.15	345	403	495	644	978	183	91	232	113	294	145	388	191	591	294
25	26.92	1.14	365	422	513	718	1003	194	95	246	122	304	151	432	214	606	303
25	25.35	1.14	364	415	512	682	989	191	95	242	117	302	150	410	202	602	299
25	24.21	1.13	349	405	489	641	968	183	92	236	116	289	141	385	190	584	290
25	23.52	1.11	322	377	461	644	944	170	83	219	107	273	136	386	191	572	286
25	22.20	1.14	331	365	450	621	923	175	88	210	104	267	131	373	183	561	279
25	20.54	1.11	294	333	405	544	821	157	78	190	95	240	119	327	163	498	245
25	18.35	1.13	259	304	377	506	788	136	68	173	87	223	111	304	151	479	237
25	15.64	1.11	233	278	344	472	722	124	62	158	79	203	102	284	141	436	217
25	13.98	1.11	222	261	316	416	633	118	58	151	74	188	93	251	124	384	189
25	12.24	1.21	205	247	295	392	578	108	53	144	71	175	86	235	116	351	174
25	10.49	1.19	179	214	274	357	524	95	48	123	61	162	80	215	107	319	158
25	9.18	1.19	167	190	238	321	454	89	43	108	54	141	70	193	95	275	137
25	7.87	1.19	143	173	208	274	387	75	38	99	49	123	61	165	82	234	116
25	6.29	1.19	119	143	179	232	333	63	30	83	41	106	53	140	69	203	100
25	5.07	1.19	107	129	155	202	262	57	27	75	37	92	46	122	60	159	79
25	3.93	1.16	87	102	125	168	212	45	23	58	30	74	36	101	50	129	64
25	3.32	1.16	70	85	102	133	174	37	19	49	25	60	30	80	39	105	52
25	2.45	1.16	58	67	85	108	143	31	15	38	19	50	25	65	31	87	44
25	1.87	1.16	44	56	67	87	110	23	11	32	16	40	20	52	26	67	33

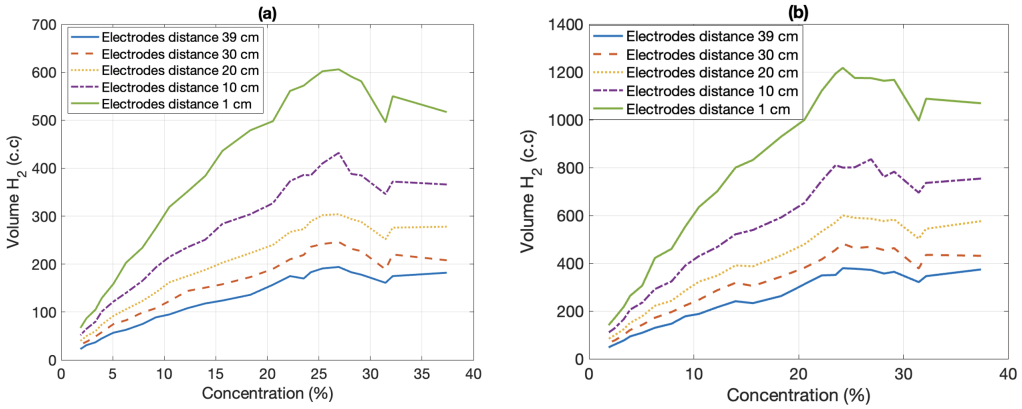

Figure 6. Hydrogen production with H_2SO_4 electrolyte volume 2lt, and stainless steel electrodes: (**a**) electrode area 50 cm^2, (**b**) electrode area 100 cm^2.

Finally, in Figure 7, the three electrolytes under experimentation, $NaHCO_3$, NaOH, and H_2SO_4, are synthesized. The experimental results indicate that the best electrolyte is sulfuric acid, with a 1 cm electrode spacing, an electrode area of 100 cm^2 each, and a hydrogen production of 1217 cc. The lowest quality electrolyte was sodium bicarbonate ($NaHCO_3$). From the practices, it was determined that hydrogen production is also proportional to the electrode area; for example, with NaOH, an electrode area of 50 cm^2 produces 298 cc, while an area of 100 cm^2 produces 596 cc of hydrogen.

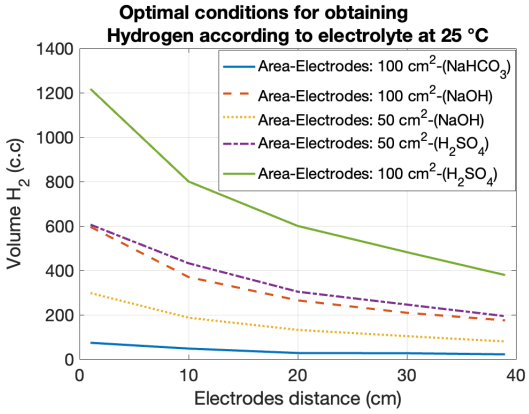

Figure 7. Optimal conditions for obtaining hydrogen with the electrolyte at 25 °C.

4. Simulation Results and Discussion

4.1. Micro-Grid Case Study

The following Figure 8 details the micro-grid equipment used in this study, which is part of the Micro-Grid Laboratory of the Universidad de Cuenca, Ecuador. It consists of a 15 kW PV system with 60 modules from the Atersa brand (Elecnor, Valencia, Spain), Samsung 44 kWh lithium batteries (Samsung, Gyeonggi-do, Republic of Korea) as the ESS, includes a 2-level bi-directional power converter, GPTech (Spain), and the Heliocentris EL500 electrolyzer (Italy) (see Tables 2 and 3), which produces 500 Nl/h at a pressure of 30 bar, with a purity of 99.94% from distilled water and a constant load of 2.39 kW to the PCC with the electrical grid. The hydrogen produced as compressed gas is stored in four tanks (50 L each) at a maximum pressure of 200 bars (Spain) [27].

The data for this simulation are presented in the following table.

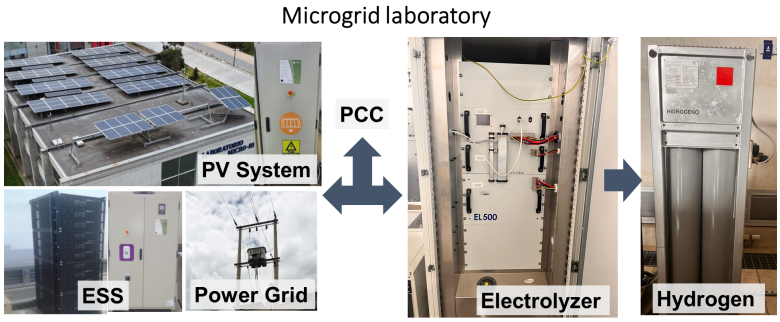

Figure 8. Case study at the Micro-Grid Laboratory, Universidad de Cuenca, Ecuador.

Table 2. Integrated micro-grid equipment.

Description	Parameter Value	Unit
PV System (60 modules 15 × 4 array)	15	kW
Lithium battery bank (11 Cells)	44	kWh
EL500 electrolyzer	2.39	kW
Bi-directional inverter	500 Vdc/230 Vac	V
Power grid	150	kVA
Storage tanks (4 × 50 L)	200	bars

Table 3. Hydrogen production data and equipment parameters.

Description	Parameter Value	Unit
Type of Electrolyzer	1	PEM
H_2 production rate	8.33	L/min
Working pressure	30	bar
Water consumption	0.4	L/h
Water specification	10	µS/cm
Power supply options	AC 220 V–50 Hz DC 40 V–80 V	V
Operative power consumption	2390	W
Universal gas constant R	0.082	L·atm/mol·K
Voltage supply	48	V
Current density	0.2	A/cm^2
Temperature	298	K
Number of cells	72	
Faraday's constant	96,485	C/mol
Electrochemical equivalent	2	cm
Area	76.1362	cm^2
Current I	15.2272	A
Voltage cell	2.4	V
Ohmic resistance of electrolyte R_u	8.05×10^{-5}	$\Omega \cdot m^2$
Ohmic resistance of electrolyte R_d	-2.5×10^{-7}	$\Omega \cdot m^2$
Over temperature shut down	65	°C
V_{ohmic}	0.1486	V
System efficiency	60 to 80	%

The following Algorithm 1 details the steps and configuration for energy control and management. The input parameters to the algorithm required as the measurement points are established according to the scheme in Figure 1. For this, the Modbus communication stations of the equipment must be initialized at a set time. Subsequently, these values are read and processed in real time for the reference values towards the ESS inverter [27,38]. The SoC control limits the energy delivery capacity autonomously, thus offering security during the management system. The system response is practically instantaneous, so the PV energy is stored in the ESS after covering the demand of the electrolyzer.

Algorithm 1 Steps and configuration for energy control and management

1: Data input: P_t^{PV}, P_t^{ETZ}, P_t^{ESS}, SoC_t^{ESS}
2: **while:** $t = 1 : N$ iteration
3: Start
4: TimerVal = tic
5: Start Modbus communication
6: m = modbus(Transport, 'Port', Name, Value)
7: Read data from a Modbus server
8: read(m, target, address, count, serverId, precision)
9: $P_t^{ref} = P_t^{PV} - P_t^{ETZ}$ Equation (3)
10: **If** $SoC_{min} \leq SoC_t^{ESS} \leq SoC_{max}$
11: $P_t^{ESS} = P_t^{ref}$ Equation (6)
12: **else**
13: $P_t^{ESS} = 0$ Equation (6)
14: **end**
15: Perform a write operation to the connected
16: Modbus server ESS value
17: write(m, target, address, values, serverId, 'precision')
18: **end**

4.2. Techno-Economic Optimization

In this section, the simulation results are presented according to the scheme in Figure 1 for the production of green hydrogen. In the simulator configuration, steps of minutes, hours, and days are added. The equipment used for the simulation was OPAL-RT Real-Time Simulation (Montreal, QC, Canada), integrating a 4-core, 3.7 GHz, 16 GB RAM, 250 GB SSD Intel® Xeon® E3 computer [39], in which a 2.39 kW electrolyzer profile and a 15 kWp photovoltaic system were assigned. The specific considerations for the technical–economic analysis are as follows:

- Annual input database of solar irradiation, temperature, and maximum storage energy.
- Conducted across a long duration of time at regular intervals ranging from 1 min to 1 h.
- Relies on steady-state operational conditions at each time interval instead of system dynamics.
- Uses a quasi-steady-state simulation.
- Effect of fluctuating PV power as a function of solar irradiation and response of power converters.
- Restriction of battery state of charge based on maximum operating capacity.
- Operating condition of the electrolyzer for 16 h without interruption.

4.2.1. Simulation with Hourly Step Configuration

During the operational simulation of the step-based system configured per hour, the electrical parameters of voltage (V), current (A), and power (kW) were recorded at the different measurement points. Figure 9a,b show the results at the PV system output points and electrolyzer demand, respectively, where a constant voltage can be observed on the 230 Vac in the PCC three-phase system (V_{R-S-T}). In Figure 9a, the PV system current responds almost proportionally to solar irradiation and power as the product of voltage and current. In addition, the electrolyzer current (I_{R-S-T}) remains practically constant due to the consumption of 2.39 kW over 16 continuous hours (see Figure 9b).

On the other hand, Figure 9c,d show the voltage, current, and power at the other measurement points of the energy storage and utility grid, respectively, where a negative power value indicates the support of the electrical grid or the discharge of the ESS; on the contrary, a positive value is the delivery of excess power to the grid or the charge of the ESS (see Figure 9c). In this case, zero consumption from the electrical grid can be seen in Figure 9d. Therefore, the system remains in generation with self-consumption.

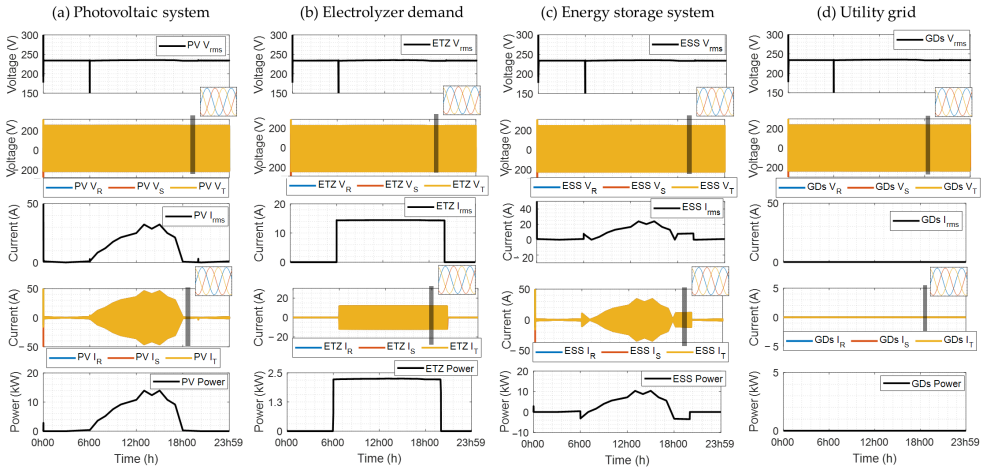

Figure 9. Simulation results: (**a**) PV system, (**b**) electrolyzer demand, (**c**) energy storage, and (**d**) utility grid with step of hours.

4.2.2. Simulation with Steps per Minute Configuration

The simulation results of the system based on steps configured per minute are presented in the following Figure 10. As can be seen, the sampling frequency of the system allows for a detailed analysis of changes in solar irradiation (see Figure 10a), which was not visible in the previous figure. The system response is coupled to more precise and optimal results for controller design and validation. However, the simulation time increases significantly. The parameters in Figure 10b do not show significant changes due to their constant electrolyzer demand value. However, the voltage level generates a variation due to the fluctuating penetration of the PV system. This directly affects all measurement points at PCC.

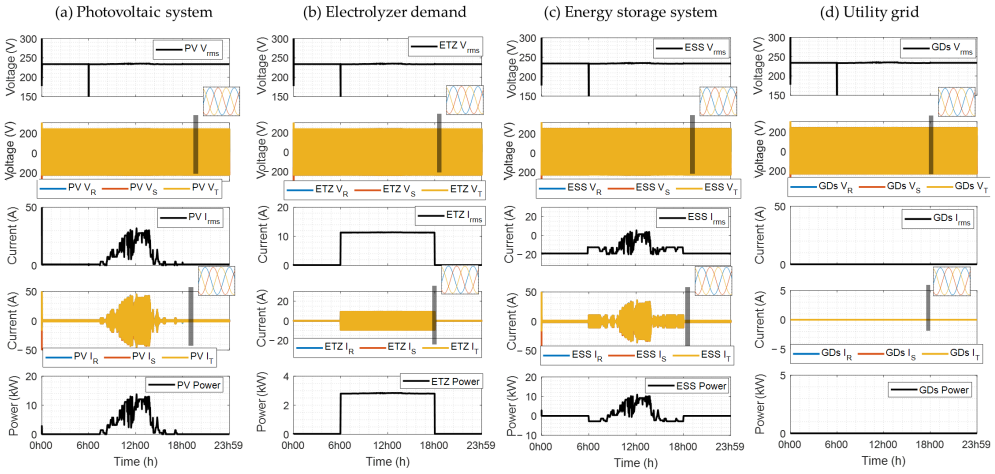

Figure 10. Simulation results: (**a**) PV system, (**b**) electrolyzer demand, (**c**) energy storage, and (**d**) utility grid with step of minutes.

Additionally, Figure 10c shows the simulation results at the ESS output, so it can be seen that the power that exceeds generation allows the charging of the ESS with $P_t^{ESS} < 0$. On the other hand, if the PV power is less than the electrolyzer demand, the batteries are discharged, delivering power to the grid, i.e., $P_t^{ESS} > 0$. In parallel, Figure 10d shows the null response from the utility grid due to the support of the PV system and the ESS. Voltage regulation can also be observed in PCC due to ESS support.

4.2.3. Simulation with Step Configuration by Months

Therefore, to demonstrate the feasibility, an analysis in steps of months is carried out for hydrogen production with the support of PV and ESS systems. In this context, an

annual database is required for the technical–economic analysis. The data corresponding to the PV production and electrolyzer demand of one year in steps of minutes are presented in the following Figure 11.

The highest PV energy production is recorded during March, September, and October, and the lowest production months are June and December. Then, considering a constant electrolyzer load of 2.39 kW during the 16 h of operation, it requires an approximate monthly energy of 1147.2 kWh/month. Finally, the viability of the system can be related to PV production and the demand for the electrolyzer during the year. These values are presented in the following Figure 12.

As can be seen, during the ten months, the electrolyzer's demand is fully supplied, and the months of lower production (June and December) require energy from the grid. This results in a model with high expectations for the production of green hydrogen.

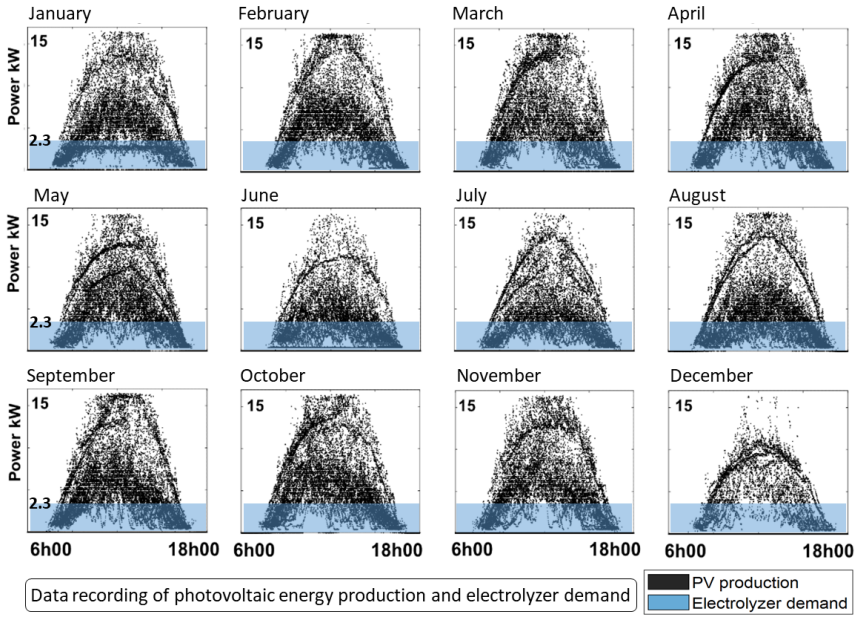

Figure 11. Monthly PV energy production and electrolyzer demand with step of minutes.

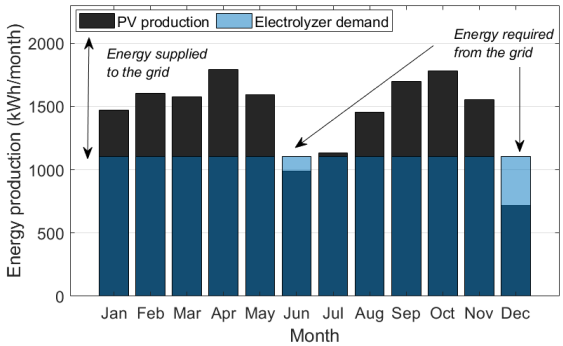

Figure 12. PV energy produced and demand of the electrolyzer monthly.

4.3. Analysis of Seasonal and Diurnal Variations in PV Performance

The variability of PV power is a crucial aspect to consider during solar power generation. This variability is influenced by weather conditions, the geographical location of the installation, and the times of day. The intermittency of solar radiation can cause these fluctuations in energy production. Therefore, in this section, the PV production versus hydrogen production is analyzed under three different climatic conditions. As mentioned above, green hydrogen production is carried out uninterruptedly. Therefore, the energy management system must maintain balance with the demand of the electrolyzer. As can be

seen in the following Figure 13, the battery support allows for optimal energy distribution with minimum consumption from the electrical grid.

Figure 13a shows a medium variability in PV production, which has generated around 50 kWh against the 38.24 kWh required by the electrolyzer. The excess value of 23.5% has been supplied to the grid. In this case, the battery SoC has started at its low value, so during the first few hours, it reaches its minimum value and requires energy from the grid. As PV production increases throughout the day, the batteries store the excess energy for discharge during the night hours. On the other hand, in the second case, the variability of the PV production is high (see Figure 13b). The PV energy reaches 65 kWh, which is about 70% of what can be delivered to the grid. Due to the conditions of this day, the energy from the grid is not required and 55% is available in the SoC. Finally, in Figure 13c, a low variability in the PV production is presented, with the energy produced during this day being 62 kWh. Unlike the first case, the state of charge reaches values higher than 60% compared to 35% in the first case. It is worth mentioning that the values are limited by the storage capacity according to Figure 5, so the algorithm must respond to the SoC of the ESS. That is, if the reference power exceeds the SoC values, the power of the ESS must be 0. This can be seen in detail in the enlargement of Figure 13c.

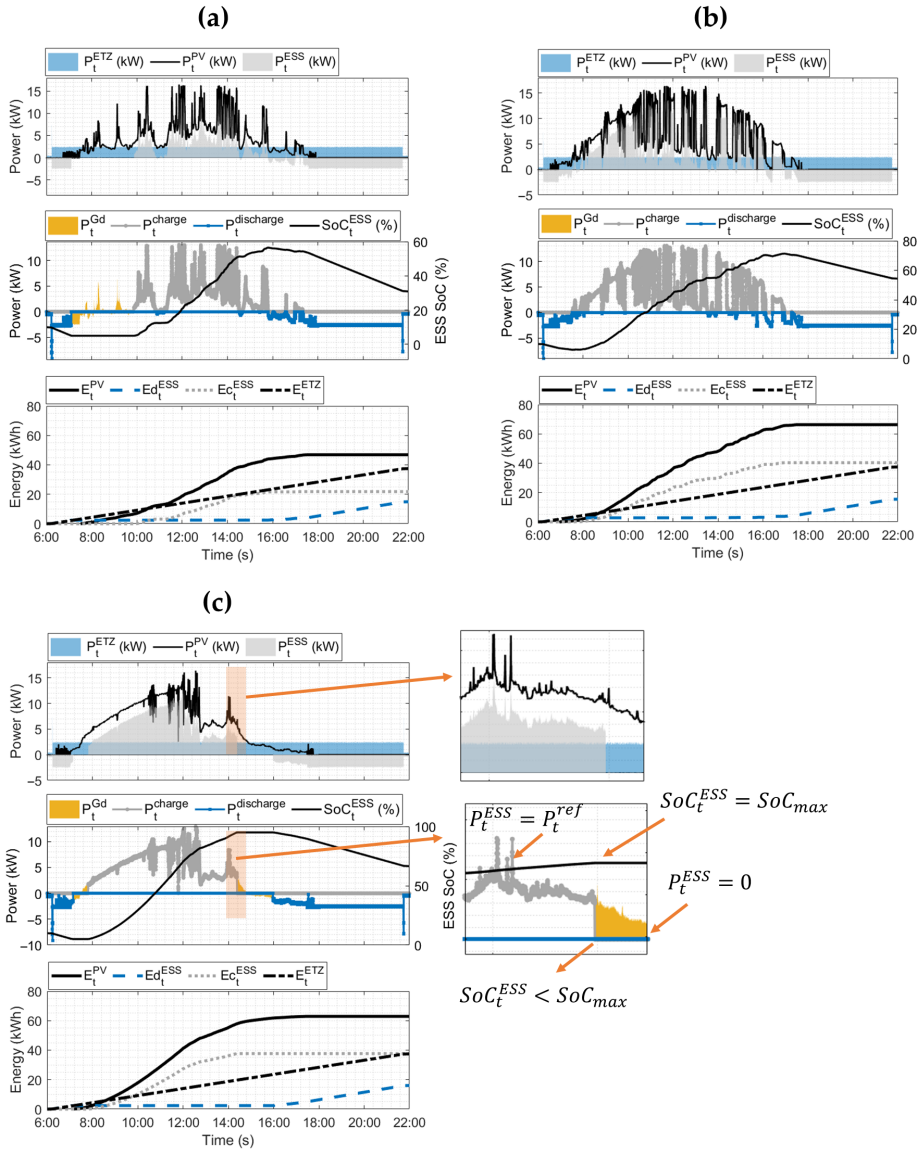

Figure 13. Analysis of seasonal variations in PV system: (**a**) medium variability, (**b**) high variability, (**c**) low variability.

4.4. Validation of Simulation Models Through Experimental Data

The following Figure 14 presents the details of experimental verification for the energy systems as a function of power. As can be observed, the variability of the PV system is due to the fact that the reference values for the model are solar radiation and ambient temperature. A scatter diagram has been included to verify the relationship between the simulation values and the real-time data. Similarly, the response time of the ESS to the variability of the PV power in the charging cycles is observed. The surplus of this energy is stored to be discharged during the night hours. In the latter case, the power response of the electrolyzer is practically a constant value during its operation; however, being a load connection/disconnection device, it causes a very short-duration transient effect. This effect is also absorbed directly by the ESS, which does not cause disturbances in the electrical grid. It should be noted that since these are low rate of change values, the scatter diagram adjusts the largest amount to 2.39 kW.

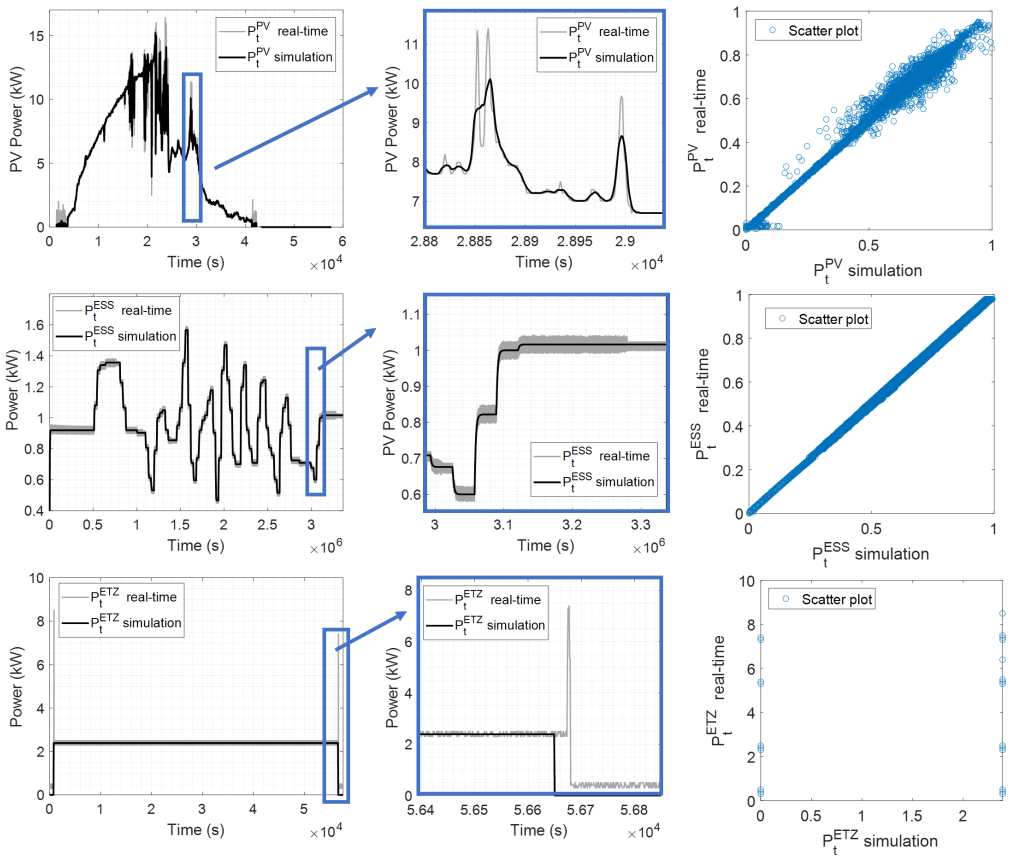

Figure 14. Validation of simulation models through experimental data.

4.5. Cost Analysis and Economic Feasibility

The price of producing green hydrogen is a key aspect for its large-scale adoption. Based on the simulations conducted according to Table 4, the results indicate that the energy consumption to produce one kilogram of hydrogen is 64 kWh. Additionally, the hydrogen production per day and year is 0.287 kg/day and 103.32 kg/year, respectively. On the other hand, a cost of 0.06 USD/day and 36 USD/year was considered as a reference for the price of water in the city of Cuenca, Ecuador. In this case, the required water consumption is 0.4 L per hour.

As shown in Figure 15a, the electrolyzer produces 0.287 kg of hydrogen per day while operating. It is important to note that the electrolyzer runs for 16 h per day and remains off for the remaining 8 h. Therefore, in this case study, the electrolyzer will produce a total of 103.32 kg of hydrogen annually.

Table 4. Costs and results from production.

Description	Parameter Value	Unit
Consumption of energy to produce hydrogen	64	kWh/kg
Production of hydrogen per day	0.287	kg/day
Production of hydrogen per year	103.32	kg/year
Cost of using water	0.06	USD/day
Cost of using water	36	USD/year
Water consumption	0.4	L/h
Water specification	10	uS/cm

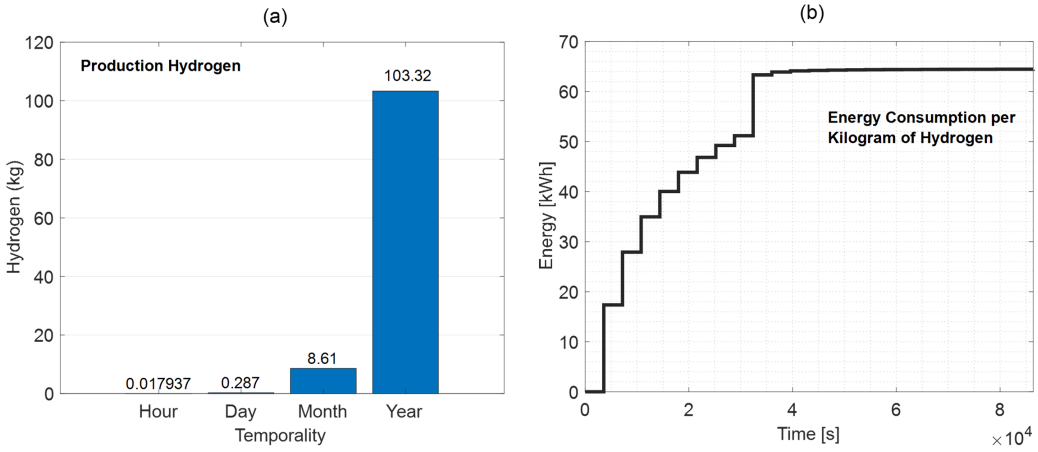

Figure 15. (**a**) Hydrogen production over time: daily to yearly. (**b**) Energy consumption per kilogram of hydrogen (kWh/kg).

In addition, based on Figure 15b, the energy consumption to produce 1 kg of hydrogen is expected to stabilize at 64 kWh after the first 9 h. In this case study, conducted in the city of Cuenca, Ecuador, where the cost of electricity is USD 0.09 per kWh, the production cost for one kilogram of hydrogen would be approximately USD 5.76.

Tables 5 and 6 present the electricity prices per hour in Ecuador for residential, commercial, and industrial consumers [40]. Consequently, the EL-500 electrolyzer consumes 2.382 kWh when operated for 16 h per day, resulting in a total daily demand of 38.08 kWh. Considering the manufacturer's reported efficiency range of 60% to 80%, the net energy consumption is between 22.08 kWh and 30.46 kWh. Additionally, during the experimental phase, it was observed that hydrogen storage at 200 bar in a 50-liter tank provided 8.919 kWh over 3 h, 27 min, and 59 s, When the fuel cell is operating at nominal power with the characteristics of Table 7 of the Ecobox-MR30S1 model (Singapore). This corresponds to a round-trip efficiency of 40.45%, which aligns with values reported in the literature [41].

Table 5. Hourly rate schemes and voltage levels.

Category	Voltage Level	Consumer Group	Demand Registration
Residential	Low Voltage LV <600 V	Residential	No demand
		Commercial	No demand With demand With hourly demand
		Industrial	No demand With demand With hourly demand

Table 6. Electricity prices hour for Ecuador.

Consumption Range (kWh)	Energy Cost (USD/kWh)	Distribution (USD/Costumer)
1 to 50	0.091	
51 to 100	0.0931	
101 to 150	0.095	
151 to 200	0.097	
201 to 250	0.099	
251 to 300	0.101	
301 to 350	0.103	1.414
351 to 500	0.105	
501 to 700	0.1285	
701 to 1000	0.1450	
1001 to 1500	0.1709	
1501 to 2500	0.2752	
2501 to 3500	0.4360	
Greater than 3501	0.6812	

Table 7. Fuel cell Ecobox-MR30S1.

Description	Parameter Value	Unit
Power Rating	0 to 3000	W
Current Rating	0 to 56	A
Voltage Adjustable	43.2 to 57.6	VDC
Voltage Ripple	± 1	V
Ambient Temperature	-10 to 45	Centigrates
Relative Humidity	0 to 95%	Non-condensing
Consumption	≤ 0.78	$\frac{Nm^3}{kWh}$
Efficiency of System	$\geq 42\%$	N/A

4.6. Analysis Considering CAPEX and OPEX

The analysis of capital expenditure (CAPEX) and operating expenditure (OPEX) is a fundamental practice in the economic evaluation of projects. Table 8 shows all the information required for the calculation of capital and operating costs.

Table 8. Cash flow: CAPEX and OPEX.

System Type	Model	Cells/Modules	Capacity	Unit Price	Capital Cost
PV	A-250P GSE Atersa	60	15 kW	800 USD/kW	12,000 USD
Electrolyzer	EL500 Acta S.p.A	1	2.3 kW	588 USD/kW	1352.4 USD
Battery	Lithium battery bank	11 Cells	44 kWh	290 USD/kWh	12,840 USD
Total Capital Cost					26,192.4 USD
Operating cost	For one year				
Labor	0.3% of total capital cost	1			78.57 USD/year
Distilled water	Ecuador distilled	1	0.4 L/H	0.66 USD/L	1520 USD/year
Maintenance	2% of total capital cost	1			523.84 USD/year
Total operating cost		1			2122.41 USD/year

Based on the values in Table 6 and Figure 12, the profit from the sale of energy to the Ecuadorian electrical system is calculated. These results are presented in the following Figure 16. As can be seen, there is a surplus in energy sales in most months, except in June and December, when additional energy must be purchased from the grid. Annual revenue from electricity sales amounts to $367.63.

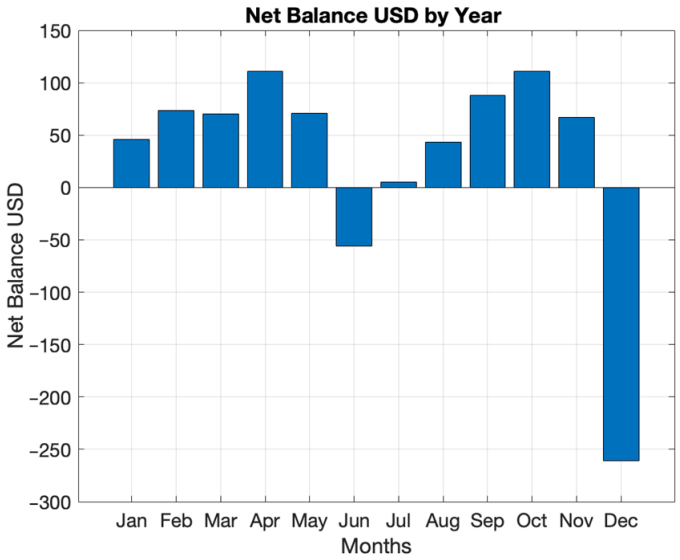

Figure 16. Net cost in the annual energy balance.

Using the cash flow balance and net income from energy sales, the annual cost of the hydrogen production project is calculated according to Equation (30):

$$\begin{aligned} \text{Total Annual Cost (year)} &= \text{Capital Cost} + \text{Annual Operatings Cost} \\ &\quad - \text{Annual Grid Revenue} \\ \text{Total Annual Cost (year)} &= \$\,26192.4 + \$\,2122.41 - \$\,367.62 = \$\,27947.19 \end{aligned} \tag{30}$$

Considering capital costs along with operation and maintenance expenses, the cost per kilogram of hydrogen is approximately

$$\begin{aligned} \text{Unit } H_2 \text{ production Cost} &= \frac{\text{Total anuual Cost}}{\text{Annual } H_2 \text{ Production}} \\ \text{Unit } H_2 \text{ production Cost} &= \frac{27947.19}{103.32 \text{ kg}} \\ \text{Unit } H_2 \text{ production Cost} &= \$\,270/\text{kg} \end{aligned} \tag{31}$$

In assessing the economic viability of hydrogen production, the levelized cost of hydrogen (LCOH) based on Equation (32) is used to calculate the average cost of hydrogen production over the entire life of the project. This includes capital, operation, and maintenance costs, as well as the cost of necessary inputs such as electricity and water.

$$\begin{aligned} \text{LCOH} &= \frac{\text{Net Present Value of total Cost (CAPEX plus OPEX) over the lifetime of the plant}}{\text{Net Present Value of total hydrogen production over the lifetime}} \\ &= \frac{27947.19}{103.32 \times 25} = \frac{\$10.81}{\text{kg}} \end{aligned} \tag{32}$$

Over the 25-year lifetime, the levelized cost of hydrogen under these conditions is compared with international hydrogen production markets. To overcome these limitations, the authors propose the following strategies.

4.6.1. Strategy 1: Offer Subsidy for Green Hydrogen Production

This strategy will enable the Ecuadorian state, through regulatory and control agencies, to analyze the appropriate price to be paid for photovoltaic generation in the production of green hydrogen (Figure 17).

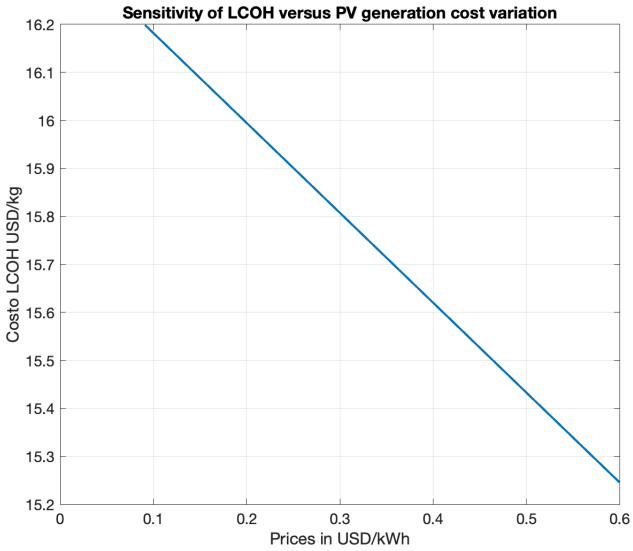

Figure 17. Sensitivity of LCOH versus PV generation cost variation.

4.6.2. Strategy 2: Variable Price per kW for the Electrolyzer

The second strategy involves maintaining an average price of 0.35 cUSD/kWh while varying the price per kW for the electrolyzer (Figure 18).

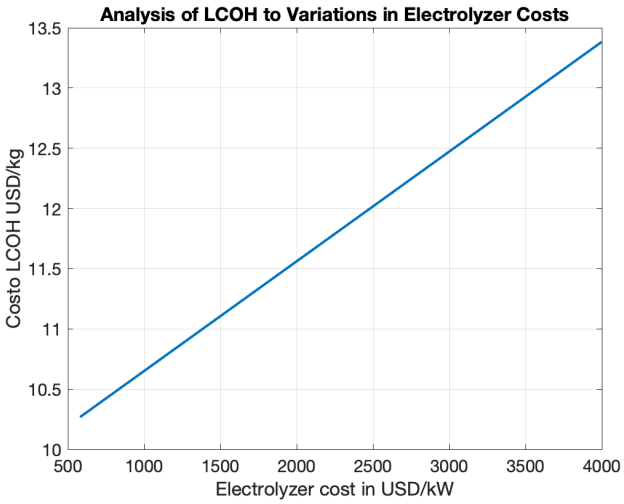

Figure 18. Analysis of LCOH versus variations in electrolyzer costs.

4.7. Comparative of Hydrogen Using Natural Gas

On the other hand, a comparative analysis has been carried out on the production of hydrogen from natural gas. For this purpose, the process was modeled through steam methane reforming, which is the most common method for producing hydrogen from natural gas, which involves two main reactions:

1.—Methane reforming:

$$CH_4 + H_2O \rightarrow CO + 3H_2 \quad (33)$$

2.—Water–gas shift reaction (optional):

$$CO + H_2O \rightarrow CO_2 + H_2 \quad (34)$$

Using the molecular weight of hydrogen $M_{H_2} = 2.016 \frac{g}{mol}$, we convert 0.287 kg of hydrogen to moles:

$$\text{Moles of } H_2 = \frac{287 \text{ g/day}}{2.016 \text{ g/mol}} = 142.3 \text{ mols/day} \tag{35}$$

The second step was to calculate the required methane and water. Since 1 mole of methane produces 3 moles of hydrogen in the stem methane reforming (SMR) process, the amount of methane required is

$$\text{Moles of } CH_4 = \frac{\text{Moles of } H_2}{3} = \frac{142.3}{3} = 47.3 \frac{\text{moles}}{\text{day}} \tag{36}$$

The water requirement is the same as the methane requirement (based on a 1:1 stoichiometric ratio).

Figure 19 represents a simulation of hydrogen production via steam methane reforming (SMR). It can be observed that methane (CH_4), initially at approximately 50 moles, is rapidly consumed, reaching nearly zero within the first 100 s. The water (H_2O), similarly to methane, begins at around 50 moles and is consumed at a similar rate, reaching near-zero. The amount of carbon monoxide (CO) increases rapidly in the beginning but stabilizes at a constant value of approximately 37 moles after a short time. The carbon dioxide (CO_2) is produced in small amounts and stabilizes at a low concentration after an initial peak. Hydrogen is the main product of the reaction, increasing sharply in the first moments and stabilizing at around 142.36 moles, showing a successful hydrogen production via SMR, equivalent to 0.287 kg/day, which closely matches the results in Figure 15.

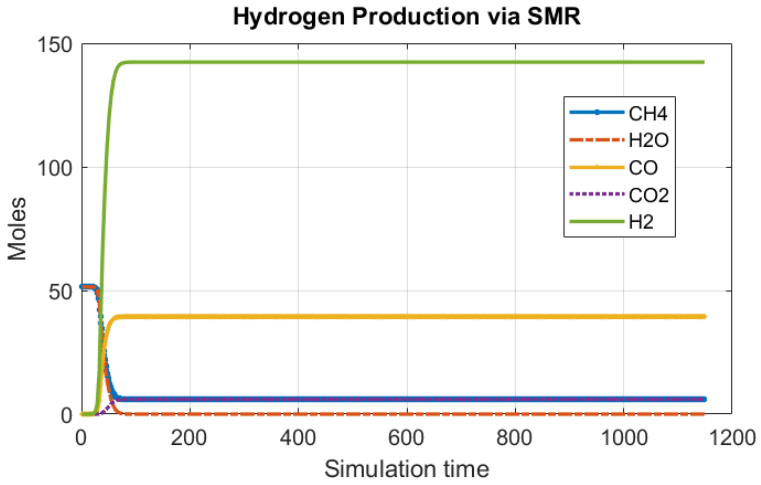

Figure 19. Energy consumption per kilogram of natural hydrogen gas as inlet.

The literature [42] indicates that hydrogen production via steam methane reforming (SMR) of natural gas (CH_4) remains the most cost-effective method for producing hydrogen gas today. Our aim in Table 9 was to make a comparison, and indeed, SMR continues to be the least expensive, even in terms of water consumption. However, it is evident that SMR has a significant environmental impact in terms of carbon emissions, an issue that photovoltaic hydrogen production mitigates entirely. In the context of Ecuador, carbon certificates can be traded, with the current price at USD 50 per ton of CO_2, providing an estimated USD 950 to avoid 19 tons of carbon emissions per year.

Table 9. Comparative hydrogen production with methane reforming SMR vs. PV generation.

Description	SMR Value	Proposal	Literature
Moles (mols/day)	47.3 (CH_4)	143.2 (H_2)	
Water	47.3 mols/day	355.5 mols/day	
(CO_2) emissions in tons in 25 years	19	0	[42]
Heat water to 1000 °C	1.034 kWh	0	
Required energy	18.194 kWh per day	38.9 KWh per day	

However, if we calculate the return on investment through carbon certificates at Ecuador's prices, we obtain an approximate payback period of 1.17 years under this mechanism as shown in the following Equation (37):

$$\begin{aligned} \text{Carbon certificate price (CCP)} &= 50 \text{ USD} \\ \text{Total Annual Cost (TAC)} &= 27947.9 \text{ USD} \\ \text{Mitigated Carbon Emissions (MCE)} &= 19 \text{ Tons} \\ \text{project lifetime (PL)} &= 25 \text{ year} \\ \text{Return on Investment} &= \frac{\text{TAC}}{\text{CCP} \times \text{MCE} \times \text{PL}} \\ &= \frac{27947.19}{50 \times 19 \times 25} = 1.17 \text{ years} \end{aligned} \tag{37}$$

4.8. Types of Models in Technology Readiness Levels

Finally, a comparative table of types of models in technology readiness levels applied to reliability in green hydrogen is established. These levels help to identify the development status of different technologies and processes during the simulation. Consequently, they allow the evaluation and planning of the development of green hydrogen technologies for future applications. Table 10 summarizes the relevant points for the selection and type of simulation required under different configurations and analysis of the results of the system modeling.

Table 10. Discussion of the types of models in TRLs.

Types of Models in TRLs	Characteristics
Techno-Economic Optimization	Execution times: 86,400 s/day, 1440 m/day, 24 h/day (monthly analysis). Step configuration: 86,400 s, 1440 m, 24 h. Advantages: Perform feasibility analysis prior to equipment acquisition. Energy feasibility studies based on renewable resources. Low computational performance in simulations. Basic software. Requirement of databases with variable sampling. Ideal for generating budgets. Disadvantages: Results generated are approximate. At the design level, it can generate unforeseen events. Limited simulation events.
Detailed Technical Design	Execution times: ns, µs, ms Step configuration: 50 µs Advantages: Real operating environments. Optimization in control drivers. Power quality analysis. Technology improvement and validation. Disadvantages: High processing capacities. Requires real-time simulators. Increased simulation time.
Operational Optimization	Execution times: 86,400 s/day, 1440 m/day, 24 h/day (monthly analysis). Step configuration: 86,400 s, 1440 m, 24 h. Advantages: Conduct feasibility analysis to expand facilities. Allows for resource optimization studies. Establish economic operations and energy management. Generate long-term studies. Low computational performance in simulations. Programming control algorithms. Disadvantages: Results generated are approximate. Limitations for installed systems. Large-scale data recording requirement.

5. Conclusions

This experimental study demonstrated the impact of different electrolytes on hydrogen production efficiency, focusing particularly on sulfuric acid (H_2SO_4) at 37% concentration. Electrochemical testing, conducted in the Laboratory of the Faculty of Chemical Sciences, provided a comparative analysis using electrodes of 50 cm^2 and 100 cm^2, showing that sulfuric acid significantly enhances current density, thus optimizing hydrogen generation. The results indicate that higher electrode surface areas yield increased hydrogen output.

The production of green hydrogen based on a micro-grid with PV system support and ESS batteries allows for improving sustainability with minimum consumption from the electric grid. This article presents a technical–economic study based on a simulation model approach.

During the electrolyzer's operation, real-time simulation is necessary to de-risk overall technology development as we move closer to system deployment. In this paper, the fidelity of a hydrogen production model is analyzed under different parameterizations in the input variables.

Energy management for green hydrogen production in a micro-grid was presented as a case study. In this case, the electrolyzer's use has been optimized for 16 operating hours per day. Consequently, the micro-grid's 15 kW PV system, together with the ESS batteries, has covered the electrolyzer's annual demand (13,766.4 kWh/year). Despite having high PV generation, energy is required from the electrical grid for two months with low energy demand.

The current simulation fidelity proposal for hydrogen yields a value of 64 kWh/kg of hydrogen. Comparing this with the values reported by IRENA in 2023, which range from 46 to 66 kWh/kg, it is evident that our results fall within this established range.

In this case study conducted in the city of Cuenca, Ecuador, the subsidized electricity cost is approximately 9.20 cUSD/kWh. However, if the actual cost of electricity, which is 16.2 cUSD/kWh, were considered, the cost of producing one kilogram of hydrogen would increase significantly, from 5.76 USD/kg to 10.36 USD/kg.

Finally, using the methane reforming method for hydrogen production, 924 kWh is required to obtain 0.287 kg of hydrogen per day. In contrast, using the PV, ESS, and grid strategy, only 64 kWh is needed, which in Ecuador would represent a cost of USD 10.36/kg in our proposal, compared to USD 134/kg for the traditional method.

Author Contributions: A.C.: Visualization, Supervision, Software, Resources, Writing—Original Draft, Writing—Review and Editing, Methodology. L.I.M.-A.: Resources, Writing—Original Draft, Methodology, Investigation, Formal Analysis, Data Curation, Writing—Review and Editing, Validation. D.B.: Visualization, Supervision, Software, Resources, Writing—Original Draft, Writing—Review and Editing, Project Administration, Methodology. D.O.-C.: Resources, Writing—Original Draft, Methodology, Investigation, Formal Analysis, Data Curation, Writing—Review and Editing, Validation. M.T.-V.: Supervision, Software, Resources, Writing—Original Draft, Project Administration, Methodology, Investigation, Funding Acquisition, Visualization. W.K.M.: Resources, Writing—Original Draft, Methodology, Investigation, Formal Analysis, Data Curation, Writing—Review and Editing, Validation. F.J.: Project Administration, Methodology, Investigation, Funding Acquisition, Formal Analysis, Data Curation, Conceptualization, Visualization. All authors have read and agreed to the published version of the manuscript.

Funding: This research received no external funding.

Institutional Review Board Statement: Not applicable.

Informed Consent Statement: Not applicable.

Data Availability Statement: The original contributions presented in the study are included in the article, further inquiries can be directed to the corresponding author.

Acknowledgments: The authors wish to thank the Spanish Ministry of Science and Innovation and European Union NextGenerationEU/PRTR, under the research Project "Desarrollo de herramientas computacionales para microrredes multi-energía con vectores de electricidad, hidrógeno y gas" (TED2021-129631B-C31). The authors thank the Faculty of Engineering, Universidad de Cuenca, Ecuador, for access to the Micro-Grid Laboratory's facilities, allowing the use of its equipment, and authorizing its staff to provide the technical support necessary to carry out the experiments described in this article. This manuscript is an outcome of the research stay enjoyed by Adrian Criollo in Spain, who gratefully acknowledges Universidad de Cuenca for funding this scholarship and extends his gratitude to the Department of Electrical Engineering at Universidad of Jaén, Spain, for hosting his research stay, which was influential in developing this work.The icons used in this document were developed by Freepik, monkik, Smashicons, and Pixel perfect, from www.flaticon.com (accessed on 30 May 2024).

Conflicts of Interest: The authors declare no conflicts of interest.

References

1. Sharma, G.D.; Verma, M.; Taheri, B.; Chopra, R.; Parihar, J.S. Socio-economic aspects of hydrogen energy: An integrative review. *Technol. Forecast. Soc. Chang.* **2023**, *192*, 122574. [CrossRef]
2. Muhammed, N.S.; Gbadamosi, A.O.; Epelle, E.I.; Abdulrasheed, A.A.; Haq, B.; Patil, S.; Al-Shehri, D.; Kamal, M.S. Hydrogen production, transportation, utilization, and storage: Recent advances towards sustainable energy. *J. Energy Storage* **2023**, *73*, 109207. [CrossRef]
3. Damiri, A.P.; Stamatakis, E.; Bellas, S.; Zoulias, M.; Mitkidis, G.; Anastasiadis, A.G.; Karellas, S.; Tzamalis, G.; Stubos, A.; Tsoutsos, T. A Review of Alternative Processes for Green Hydrogen Production Focused on Generating Hydrogen from Biomass. *Hydrogen* **2024**, *5*, 163–184. [CrossRef]
4. Squadrito, G.; Maggio, G.; Nicita, A. The green hydrogen revolution. *Renew. Energy* **2023**, *216*, 119041. [CrossRef]
5. Ma, N.; Zhao, W.; Wang, W.; Li, X.; Zhou, H. Large scale of green hydrogen storage: Opportunities and challenges. *Int. J. Hydrogen Energy* **2024**, *50*, 379–396. [CrossRef]
6. Bayssi, O.; Nabil, N.; Azaroual, M.; Bousselamti, L.; Boutammachte, N.; Rachidi, S.; Barberis, S. Green hydrogen landscape in North African countries: Strengths, challenges, and future prospects. *Int. J. Hydrogen Energy* **2024**, *84*, 822–839. [CrossRef]
7. Moritz, M.; Schönfisch, M.; Schulte, S. Estimating global production and supply costs for green hydrogen and hydrogen-based green energy commodities. *Int. J. Hydrogen Energy* **2023**, *48*, 9139–9154. [CrossRef]
8. Makepeace, R.W.; Tabandeh, A.; Hossain, M.; Asaduz-Zaman, M. Techno-economic analysis of green hydrogen export. *Int. J. Hydrogen Energy* **2024**, *56*, 1183–1192. [CrossRef]
9. Hassan, Q.; Algburi, S.; Sameen, A.Z.; Salman, H.M.; Jaszczur, M. Green hydrogen: A pathway to a sustainable energy future. *Int. J. Hydrogen Energy* **2024**, *50*, 310–333. [CrossRef]
10. Mirza, U.K.; Ahmad, N.; Harijan, K.; Majeed, T. A vision for hydrogen economy in Pakistan. *Renew. Sustain. Energy Rev.* **2009**, *13*, 1111–1115. [CrossRef]
11. El-Shimy, M.; Afandi, A. Overview of Power-to-Hydrogen-to-Power (P2H2P) systems based on variable renewable sources. In Proceedings of the 5th International Conference on Electrical, Electronics, and Information Engineering, Malang, Indonesia, 6–8 October 2017; Volume 6.
12. Ngouleu, C.A.W.; Koholé, Y.W.; Fohagui, F.C.V.; Tchuen, G. Techno-economic analysis and optimal sizing of a battery-based and hydrogen-based standalone photovoltaic/wind hybrid system for rural electrification in Cameroon based on meta-heuristic techniques. *Energy Convers. Manag.* **2023**, *280*, 116794. [CrossRef]
13. Naderipour, A.; Abdul-Malek, Z.; Nowdeh, S.A.; Kamyab, H.; Ramtin, A.R.; Shahrokhi, S.; Klemeš, J.J. Comparative evaluation of hybrid photovoltaic, wind, tidal and fuel cell clean system design for different regions with remote application considering cost. *J. Clean. Prod.* **2021**, *283*, 124207. [CrossRef]
14. Kushwaha, P.K.; Bhattacharjee, C. Integrated techno-economic-enviro-socio design of the hybrid renewable energy system with suitable dispatch strategy for domestic and telecommunication load across India. *J. Energy Storage* **2022**, *55*, 105340. [CrossRef]
15. Fabianek, P.; Madlener, R. Techno-economic analysis and optimal sizing of hybrid PV-wind systems for hydrogen production by PEM electrolysis in California and Northern Germany. *Int. J. Hydrogen Energy* **2024**, *67*, 1157–1172. [CrossRef]
16. Posso, F.; Galeano, M.; Baranda, C.; Franco, D.; Rincón, A.; Zambrano, J.; Cavaliero, C.; Lópes, D. Towards the Hydrogen Economy in Paraguay: Green hydrogen production potential and end-uses. *Int. J. Hydrogen Energy* **2022**, *47*, 30027–30049. [CrossRef]
17. Ikuerowo, T.; Bade, S.O.; Akinmoladun, A.; Oni, B.A. The integration of wind and solar power to water electrolyzer for green hydrogen production. *Int. J. Hydrogen Energy* **2024**, *76*, 75–96. [CrossRef]
18. Abdelkareem, M.A.; Abdelghafar, A.A.; Mahmoud, M.; Sayed, E.T.; Mahmoud, M.S.; Alami, A.H.; Al Agha, M.M.; Olabi, A.G. Optimized solar photovoltaic-powered green hydrogen: Current status, recent advancements, and barriers. *Sol. Energy* **2023**, *265*, 112072. [CrossRef]
19. Gibson, T.L.; Kelly, N.A. Optimization of solar powered hydrogen production using photovoltaic electrolysis devices. *Int. J. Hydrogen Energy* **2008**, *33*, 5931–5940. [CrossRef]

20. Tuinema, B.W.; Adabi, E.; Ayivor, P.K.; García Suárez, V.; Liu, L.; Perilla, A.; Ahmad, Z.; Rueda Torres, J.L.; van der Meijden, M.A.; Palensky, P. Modelling of large-sized electrolysers for real-time simulation and study of the possibility of frequency support by electrolysers. *IET Gener. Transm. Distrib.* **2020**, *14*, 1985–1992. [CrossRef]
21. Dozein, M.G.; Jalali, A.; Mancarella, P. Fast frequency response from utility-scale hydrogen electrolyzers. *IEEE Trans. Sustain. Energy* **2021**, *12*, 1707–1717. [CrossRef]
22. Dozein, M.G.; De Corato, A.M.; Mancarella, P. Virtual inertia response and frequency control ancillary services from hydrogen electrolyzers. *IEEE Trans. Power Syst.* **2022**, *38*, 2447–2459. [CrossRef]
23. Dozein, M.G.; De Corato, A.M.; Mancarella, P. Fast frequency response provision from large-scale hydrogen electrolyzers considering stack voltage-current nonlinearity. In Proceedings of the 2021 IEEE Madrid PowerTech, Madrid, Spain, 28 June–2 July 2021; IEEE: Piscataway, NJ, USA, 2021; pp. 1–6.
24. Samani, A.E.; D'Amicis, A.; De Kooning, J.D.; Bozalakov, D.; Silva, P.; Vandevelde, L. Grid balancing with a large-scale electrolyser providing primary reserve. *IET Renew. Power Gener.* **2020**, *14*, 3070–3078. [CrossRef]
25. Conn, A.R.; Gould, N.I.; Toint, P.L. *Trust Region Methods*; SIAM: Philadelphia, PA, USA, 2000.
26. Misener, R.; Biegler, L. Formulating data-driven surrogate models for process optimization. *Comput. Chem. Eng.* **2023**, *179*, 108411. [CrossRef]
27. Espinoza, J.; Gonzalez, L.; Sempertegui, R. Micro grid laboratory as a tool for research on non-conventional energy sources in Ecuador. In Proceedings of the 2017 IEEE International Autumn Meeting on Power, Electronics and Computing (ROPEC), Ixtapa, Mexico, 8–10 November 2017; IEEE: Piscataway, NJ, USA, 2017; pp. 1–7.
28. Benavides Padilla, D.J.; Jurado, F.; González, L.G. Data analysis and tools applied to modeling and simulation of a PV system in Ecuador. *Enfoque UTE* **2018**, *9*, 1–12. [CrossRef]
29. Markvart, T.; Castañer, L. Chapter IA-1—Principles of Solar Cell Operation. In *Practical Handbook of Photovoltaics*, 2nd ed.; McEvoy, A., Markvart, T., Castañer, L., Eds.; Academic Press: Boston, MA, USA, 2012; pp. 7–31. [CrossRef]
30. Schalenbach, M.; Zeradjanin, A.R.; Kasian, O.; Cherevko, S.; Mayrhofer, K.J. A Perspective on Low-Temperature Water Electrolysis – Challenges in Alkaline and Acidic Technology. *Int. J. Electrochem. Sci.* **2018**, *13*, 1173–1226. [CrossRef]
31. Tremblay, O.; Dessaint, L.A. A generic fuel cell model for the simulation of fuel cell vehicles. In Proceedings of the 2009 IEEE Vehicle Power and Propulsion Conference, Dearborn, MI, USA, 7–10 September 2009; IEEE: Piscataway, NJ, USA, 2009; pp. 1722–1729.
32. Liu, H.; Zhou, T. CFD based PEM fuelcell models and applications. In Proceedings of the Technical Proceedings of the 2003 Nanotechnology Conference and Trade Show, San Francisco, CA, USA, 23–27 February 2003; Volume 3, pp. 463–466.
33. Yu, Q.; Srivastava, A.K.; Choe, S.Y.; Gao, W. Improved modeling and control of a PEM fuel cell power system for vehicles. In Proceedings of the Proceedings of the IEEE SoutheastCon 2006, Memphis, TN, USA, 31 March–2 April 2006; IEEE: Piscataway, NJ, USA, 2006; pp. 331–336.
34. O'hayre, R.; Cha, S.W.; Colella, W.; Prinz, F.B. *Fuel Cell Fundamentals*; John Wiley & Sons: Hoboken, NJ, USA, 2016.
35. Kim, M.J.; Peng, H.; Lin, C.C.; Stamos, E.; Tran, D. Testing, modeling, and control of a fuel cell hybrid vehicle. In Proceedings of the 2005 American Control Conference, Portland, OR, USA , 8–10 June 2005; IEEE: Piscataway, NJ, USA, 2005; pp. 3859–3864.
36. Acharya, P.; Enjeti, P.; Pitel, I.J. An advanced fuel cell simulator. In Proceedings of the Nineteenth Annual IEEE Applied Power Electronics Conference and Exposition, 2004. APEC'04, Anaheim, CA, USA, 22–26 February 2004; IEEE: Piscataway, NJ, USA, 2004; Volume 3, pp. 1554–1558.
37. Veintimilla, N.A.; Salazar, L.A.G. Obtaining Combustible Hydrogen by Electrolysis of Water, Using Photovoltaic Panels. Bachelor's Thesis, Cuenca, Spain, 2008. Available online: https://dspace.ucuenca.edu.ec/handle/123456789/8378 (accessed on 10 November 2024). (In Spanish)
38. Benavides, D.; Arévalo, P.; Ortega, A.C.; Sánchez-Sutil, F.; Villa-Ávila, E. Energy Management Model for a Remote Microgrid Based on Demand-Side Energy Control. *Energies* **2024**, *17*, 170. [CrossRef]
39. Benavides, D.; Arévalo, P.; Criollo, A.; Tostado-Véliz, M.; Jurado, F. Multi-mode monitoring and energy management for photovoltaic-storage systems. *Renew. Energy* **2024**, *230*, 120820. [CrossRef]
40. *Resolución ARCERNNR-021-2021: Costos SPEE 2022*; Agencia de Regulación y Control de Energía: Quito, Ecuador, 2022.
41. Ho, C.K.; Ambrosini, A. Thermal energy storage technologies. In *The 2020 US Department of Energy (DOE) Energy Storage Handbook (ESHB)*; DOE: Washington, DC, USA, 2020; pp. 162–171.
42. Nyangon, J.; Darekar, A. Advancements in hydrogen energy systems: A review of levelized costs, financial incentives and technological innovations. *Innov. Green Dev.* **2024**, *3*, 100149. [CrossRef]